First-principles aluminum database: Energetics of binary Al alloys and compounds

C. Wolverton
Ford Research and Advanced Engineering, MD3083/SRL, Dearborn, Michigan 48121-2053, USA

V. Ozoliņš
Department of Materials Science and Engineering, University of California, Los Angeles, California 90095-1595, USA
(Received 29 December 2005; published 10 April 2006)

Using an extensive series of first-principles density functional calculations, we have constructed a "first-principles aluminum database" of thermodynamic properties of binary Al-based alloys with 26 different solute elements, *X*. In all cases, first-principles results are critically compared to experimental data for observed Al-rich ordered compounds, dilute impurities in Al, disordered Al-*X* solid solutions, and pure elements, *X*, in a variety of structure types. We find the following: (i) In all Al-*X* systems, first-principles formation enthalpies of ordered compounds are in excellent agreement with experimental data. Impurity energetics for *X* in Al also agree rather well with thermodynamically assessed values from the COST507 database. (ii) Formation enthalpies of ordered compounds and energies of dilute impurities for elements from the 3*d* series are most negative at the beginning and the end of the series, and reach a maximum near the middle of the series for Cr. The ordering tendency decreases dramatically in the Al-Cu system with filled *d* bands. (iii) The special quasirandom structure approach has been used to obtain mixing energies of disordered solid solutions across the whole composition range for all systems. We find that mixing energies follow the same general trend across the 3*d* series as the ordered and impurity formation enthalpies. Asymmetry in the mixing energies is also similar in all systems, giving less negative mixing energies for Al-rich compositions. (iv) Calculation of the solubility enthalpy, which is the difference in the formation energy per solute atom between the ordered and dilute solid solution phases, shows that the observed low solubility in Al-*X* systems is due to very negative values of the ordered formation enthalpies in comparison with those for the dilute solid solution.

DOI: 10.1103/PhysRevB.73.144104 PACS number(s): 71.15.Nc, 71.20.Gj, 61.66.Dk, 61.50.Ah

I. INTRODUCTION

Understanding the complexities of phase stability in alloys is a classic problem in materials science. Aluminum and its alloys form a critical testbed on which to prove theories of phase stability due to the rich variety of ordered compounds, solid solutions, and metastable phases.[1–4] The stability of these Al-rich phases is not only of scientific but also technological interest, as understanding phase stability is a prerequisite for a systematic design and control of alloy properties.

Many computational tools have emerged to study phase stability in alloys. Two such tools are of immediate relevance to the work presented in this paper: (1) *First-principles electronic structure calculations*, based on density functional theory[5] (DFT), have become a widely used tool in the exploration of structural and alloy phase stability. Due to the predictive nature of these methods, as well as continuing improvements in physical accuracy, algorithms and computational power, first-principles methods are increasingly gaining acceptance as a powerful tool in alloy design. (2) *Calculation-of-phase-diagram (CALPHAD) methods*[6–8] use databases of thermodynamic functions and are capable of producing accurate phase diagrams and phase equilibria, even for complex multicomponent alloys, ubiquitous in practical applications. Over the course of many years, CALPHAD methods have been applied to a wide variety of commercial alloys systems and databases have been developed for a number of key alloy classes (e.g., Al-based alloys, Fe-based alloys, Mg-based alloys). However, these approaches do not *predict* new thermodynamic data and therefore are restricted to cases where thermodynamic data are already available. On the other hand, it has recently been shown[9] that first-principles methods can provide a useful complement to CALPHAD approaches by providing energetics and other thermodynamic functions in cases where experimental data are unavailable, such as the technologically important case of metastable precipitate phases.

In this paper we report on a "first-principles aluminum database" of thermodynamic and structural properties constructed via an extensive series of calculations of ordered and disordered phases. We compare in detail the results of these first-principles calculations with the experimentally well-established thermodynamic functions for these alloys. In order to facilitate the most meaningful and critical comparison with experiment, we focus on binary aluminum alloys, as these systems are the most straightforward to compute with first-principles methods and are also the ones with the best-established experimental data. In particular, we choose to carry out a detailed comparison of our first-principles results with the experimentally-assessed results from the COST507 database.[10] The COST507 database represents an extensive international European collaborative program to study lightweight alloy systems, and contains many of the binary aluminum systems considered here.

There are several rationales for performing such a study. First, this extensive first-principles investigation of thermodynamics in aluminum alloys will improve our understanding of the physics of phase stability in Al alloys. Second, by comparing our results with the well-tested and mature databases available for Al alloys, we gain confidence in the *pre-*

dictive power of first-principles methods for systems where experimental information is missing or incomplete. For instance, recent first-principles predictions in the Al-Cu system have provided surprising results in the areas of ground state stability, metastable precipitate equilibria, and precipitate morphologies.[9,11–13] A critical comparison of first-principles energetics of Al-Cu with available experimental data, such as that given here, gives us confidence in the predicted energetics for cases where experimental data do not exist. Last, this type of study should provide an avenue towards performing similar studies for emerging classes of materials, where mature CALPHAD databases are not available. These efforts could greatly accelerate the development of CALPHAD databases.

Our first-principles study consists of binary Al-X systems, for twenty-six different solutes, including most of the elements commonly found in commercial alloy systems:

(1) Period II: X=Li.

(2) Period III: X=Mg, Si.

(3) Period IV:
X=Sc, Ti, V, Cr, Mn, Fe, Co, Ni, Cu,
Zn, Ga, Ge.

(4) Period V: X=Sr, Zr, Ag, Cd, In, Sn, Sb.

(5) Period VI: X=Ba, Au, Pb, Bi.

For each of these systems, we compute the energetics and structure of several different phases: (i) the most Al-rich ordered compound observed, (ii) the dilute impurity limit, via supercells of 32 to 64 atoms, and (iii) the disordered solid solution phases using the special quasirandom structure (SQS) approach.[14] (iv) In addition, we show below that the "promotion energy," the energy required to promote each of the pure solutes from their equilibrium crystal structures to an fcc structure, provides a useful construct for analyzing the phase stability results. Therefore, we also compute the promotion energy for each of the solutes.

In this paper, we focus on the energetic quantities described above. A future paper will focus on vibrational and structural properties, thermodynamics, and solubility in Al-alloy systems.

II. METHODOLOGY

A. First-principles method

The first-principles calculations described below utilize the plane wave pseudopotential method, as implemented in the highly efficient Vienna *ab initio* simulation package (VASP).[15] In the vast majority of calculations, we used ultrasoft pseudopotentials (US), but we also performed a few comparisons with projector augmented wave (PAW) method.[16,17] Both the local density approximation (LDA) and the generalized gradient approximation (GGA) were used, with the exchange-correlation functionals of Ceperley and Alder,[18,19] and Perdew and Wang,[20] respectively. Results concerning comparisons of LDA and GGA will be discussed below. For calculations involving magnetic 3d elements Cr, Mn, Fe, Co, and Ni, spin-polarized calculations were also performed. Tests were performed for the early transition elements, Sc and Ti, treating 3p electrons as valence vs core, with only small differences found between the two sets of calculations. All structures were fully relaxed with respect to volume as well as all cell-internal and -external coordinates.

We have studied the convergence properties of the energetic calculations with respect to energy cutoff, **k**-point sampling, as well as (in the case of impurity energies) supercell size. We find converged results with a relatively modest energy cutoff (237 eV) and, in the case of dilute impurities, supercell size (32 or 64 atoms). The 32-atom impurity supercells are constructed from a simple doubling of the conventional fcc cube in all directions. The 64-atom supercells are constructed by quadrupling the conventional fcc cell in all directions, and then taking a face-centered cubic translation of this quadrupled cell. For consistency, the 237 eV cutoff was used for all elements, despite the fact that it is probably overconverged for some solute elements (e.g., Mg, Si). Unless otherwise stated, all results given here are for this value of the energy cutoff and for US potentials. (For the PAW calculations described below, a cutoff of 350 eV was used.) However, we find that an extremely dense **k**-point mesh is necessary for converged energetics. For calculated results on fcc-based supercells (impurity energies, special quasirandom structures, etc.), we use equivalent[21] k-point meshes and results are given for k-point meshes equivalent to a $24\times24\times24$ grid in the fcc constituent. For non-fcc-based structures (e.g., many of the ordered compounds), we have used dense Monkhorst-Pack[22] meshes. Extensive tests of **k**-point sampling indicated that total energy differences were converged to well within 0.01 eV. Our finding of the necessity of using a dense **k**-point mesh in computing defect properties in Al is consistent with similar conclusions from previous work.[23–25]

B. Structure types: Pure elements, ordered compounds, and solution phases

For all Al-X binary systems considered, first-principles calculations were performed for the following types of cells:

Pure elements: We calculated energetics for all elements in many different crystal structure types: fcc, bcc, hcp, β-Sn, diamond, bct, as well as the observed ground state structure in all cases. Table I lists the observed structure types for each solute element X, as found in Ref. 3.

Ordered compounds: We also calculated the energetics of the most Al-rich compound observed[3] for each Al-X system. These ordered compounds are listed in Table I, and include a wide variety of structure types, local coordinations, unit cell sizes, and symmetries. These structure types range from the relatively simple structures such as AlSb, Al_2Au, and Al_3Sc, cubic compounds with 2, 3, and 4 atoms in the primitive cell to the geometrically-complex $Al_{45}V_7$ and $Al_{13}Fe_4$ phases, both monoclinic with 52 and 51 atoms per primitive cell, respectively.

Impurity supercells: We have obtained the energetics of the dilute solution phase from supercells of fcc-Al with a single substitutional impurity. These calculations were performed for cells with 32- and 64-atoms.

Special quasirandom structures (SQS): In addition to the dilute solution and ordered compound phases, it is also useful to describe the energetics of the solid solution phases for a wide range of compositions. However, describing the en-

TABLE I. Crystal structures of elements and Al-rich compounds considered in this paper, as reported in Ref. 3. Given are the structure name/stoichiometry, as well as the Strukturbericht designation (where available), Pearson symbol, and prototype. Systems in which there are no reported stable compounds are indicated by a formula of "—." (Note that for Al-Ti, Al-V, Al-Mn, and Al-Fe, several different compounds are considered, as discussed in the text.)

Solute	Pure element				Al-rich Compound			
	Structure	Strukturbericht	Pearson symbol	Prototype	Formula	Strukturbericht	Pearson symbol	Prototype
Li	hcp	*A*3	hP2	Mg	AlLi	*B*32	cF16	NaTl
Mg	hcp	*A*3	hP2	Mg	$Al_{12}Mg_{17}$	*A*12	cI58	$\sim\alpha$-Mn
Si	diamond	*A*4	cF8	C	—			
Sc	hcp	*A*3	hP2	Mg	Al_3Sc	$L1_2$	cP4	$AuCu_3$
Ti	hcp	*A*3	hP2	Mg	Al_3Ti	$D0_{22}$	tI8	Al_3Ti
					Al_3Ti	$D0_{23}$	tI16	Al_3Zr
V	bcc	*A*2	cI2	W	$Al_{10}V$	—	cF176	
					$Al_{45}V_7$	—	mC104	$Al_{45}V_7$
					Al_3V	$D0_{22}$	tI8	Al_3Ti
Cr	bcc-AFM	—			$Al_{45}Cr_7$	—	mC104	$Al_{45}V_7$
Mn	α-Mn	*A*12	cI58	Mn	$Al_{12}Mn$	—	cI26	$Al_{12}W$
					Al_6Mn	$D2_h$	oC28	Al_6Mn
Fe	bcc-FM	*A*2	cI2	W	$Al_{13}Fe_4$	—	mC102	$Al_{13}Fe_4$
					Al_6Fe	$D2_h$	oC28	Al_6Mn
					Al_9Fe_2	—	mP22	Al_9Co_2
Co	hcp-FM	*A*3	hP2	Mg	Al_9Co_2	—	mP22	Al_9Co_2
Ni	fcc-FM	*A*1	cF4	Cu	Al_3Ni	$D0_{11}$	oP16	Fe_3C
Cu	fcc	*A*1	cF4	Cu	Al_2Cu	*C*16	tI12	Al_2Cu
Zn	hcp	*A*3	hP2	Mg	—			
Ga	α-Ga	*A*11	oC8	Ga	—			
Ge	diamond	*A*4	cF8	C	—			
Sr	bcc	*A*2	cI2	W	Al_4Sr	$D1_3$	tI10	Al_4Ba
Zr	hcp	*A*3	hP2	Mg	Al_3Zr	$D0_{23}$	tI16	Al_3Zr
Ag	fcc	*A*1	cF4	Cu	AlAg[a]			
Cd	hcp	*A*3	hP2	Mg	—			
In	bct	*A*6	tI2	In	—			
Sn	β-Sn	*A*5	tI4	Sn	—			
Sb	α-As	*A*7	hR2	As	AlSb	*B*3	cF8	ZnS
Ba	bcc	*A*2	cI2	W	Al_4Ba	$D1_3$	tI10	Al_4Ba
Au	fcc	*A*1	cF4	Cu	Al_2Au	*C*1	cF12	Ca_2F
Pb	fcc	*A*1	cF4	Cu	—			
Bi	α-As	*A*7	hR2	As	—			

[a]Al_2Ag_2 superlattice stacked along [110] (see text).

ergetics of solid solutions from first-principles is problematic since these calculations are currently limited to relatively small system sizes. This problem can be overcome by using the "special quasirandom structure" (SQS) approach,[14] an efficient means to calculate random alloy properties within a small-unit-cell approach. In this paper, we use fully relaxed, binary 16-atom SQS's (described in Appendix A of Ref. 26) with stoichiometries A_3B, AB, and AB_3.

III. PHYSICAL DECOMPOSITION OF ENERGETICS

We begin with a description and physical decomposition of the energetic quantities considered here:

(a) The equilibrium formation enthalpy of a binary ordered compound is given by the total energy $E(A_pB_q)$ of the A_pB_q compound, taken with respect to equivalent amounts of the A and B constitutents, each in their equilibrium crystal structures

$$\Delta H^{\mathrm{eq}}_{\mathrm{ord}}(A_pB_q) = E(A_pB_q) - [(1-x)E^{\mathrm{eq}}(A) + xE^{\mathrm{eq}}(B)], \quad (1)$$

where the energies (per atom) of the compound and constituents are each relaxed to their equilibrium, zero-pressure geometries. x is the composition of B in the compound, $\frac{q}{p+q}$.

(b) The mixing enthalpy of the solid solution is the analo-

gous energy difference for the $A_{1-x}B_x$ disordered solution

$$\Delta H^{\mathrm{eq}}_{\mathrm{mix}}(A_{1-x}B_x) = E(A_{1-x}B_x) - [(1-x)E^{\mathrm{eq}}(A) + xE^{\mathrm{eq}}(B)]. \tag{2}$$

(In the case of this paper, we are concerned with Al-rich solutions, and therefore only consider fcc-based solution phases.)

(c) The dilute impurity energy $\Delta H^{\mathrm{eq}}_{\mathrm{imp}}$ is simply the limit of the mixing enthalpy $\Delta H^{\mathrm{eq}}_{\mathrm{mix}}$ (expressed in units of energy per solute atom) as $x \to 0$. For these energetic properties of dilute systems, we need to distinguish the difference between energy per atom and energy per solute atom

$$\Delta H^{\mathrm{eq}}(\text{per solute atom}) = \frac{1}{x}\Delta H^{\mathrm{eq}}(\text{per atom}). \tag{3}$$

From Eq. (2), one can see that $\Delta H^{\mathrm{eq}}_{\mathrm{mix}}$ expressed in terms of *energy per atom* tends to zero as $x \to 0$. However, the *energy per solute atom* does not vanish as $x \to 0$, but rather approaches the dilute impurity energy. This distinction can be simply illustrated in a graphical way: if the formation enthalpies are plotted in units of energy per atom, the dilute impurity energy is the slope of the mixing energy curve as $x \to 0$.

(d)–(f) "fcc-based" quantities: (d) formation enthalpies of ordered compounds, (e) mixing enthalpies, and (f) dilute impurity energies. The fcc-based quantities are similar to the above "equilibrium" quantities (a)–(c), but are given with respect to a reference state of constituents in the fcc structure, rather than the constituents in their equilibrium structures. For instance, for an ordered compound, Eq. (1) gives the equilibrium formation enthalpy, whereas the fcc-based formation enthalpy is given by

$$\Delta H^{\mathrm{fcc}}_{\mathrm{ord}}(A_pB_q) = E(A_pB_q) - [(1-x)E^{\mathrm{fcc}}(A) + xE^{\mathrm{fcc}}(B)]. \tag{4}$$

The reason for defining the fcc-based quantities is that in CALPHAD studies, the fcc-based mixing enthalpy of the solid solution, $\Delta H^{\mathrm{fcc}}_{\mathrm{mix}}$, is often written as a polynomial in concentration

$$\Delta H^{\mathrm{fcc}}_{\mathrm{mix}}(A_{1-x}B_x) = \sum_n L^n x(1-x)(1-2x)^n \tag{5}$$

with polynomial coefficients L^n.

To obtain the formation enthalpy with respect to the equilibrium constituents, ΔH^{eq}, from the fcc-based formation enthalpy, ΔH^{fcc}, one simply has to add the composition-weighted energy required to promote each of the constituents from the equilibrium structure to the fcc structure

$$\Delta H^{\mathrm{eq}} = \Delta H^{\mathrm{fcc}} + (1-x)[E^{\mathrm{fcc}}(A) - E^{\mathrm{eq}}(A)] + x[E^{\mathrm{fcc}}(B) - E^{\mathrm{eq}}(B)]. \tag{6}$$

(g) The promotion energy, $\Delta E_{\mathrm{promo}}$, is defined as the energy required to promote a constituent A from its equilibrium structure to the fcc structure

$$\Delta E_{\mathrm{promo}}(A) = E^{\mathrm{fcc}}(A) - E^{\mathrm{eq}}(A). \tag{7}$$

(h) The solubility enthalpy is the last quantity we consider, and is simply given by the difference (per solute atom) of the ordered and impurity formation enthalpies

$$\Delta H_{\mathrm{sol}} = \Delta H_{\mathrm{ord}}(\text{per solute atom}) - \Delta H_{\mathrm{imp}}(\text{per solute atom}). \tag{8}$$

Note that in this difference, the pure element terms subtract away, so it is not important whether the equilibrium or fcc-based quantities are used in Eq. (8). We refer to this term as the solubility enthalpy as it is the crucial energetic contribution that enters an ideal solution expression for the solubility x_0 at temperature T_0:[27]

$$x_0 = e^{\Delta H_{\mathrm{sol}}/kT_0} e^{-\Delta S_{\mathrm{sol}}/k_B}, \tag{9}$$

where ΔS_{sol} is the difference in nonconfigurational entropy (per solute atom) between the ordered and disordered states. In the case of nonmagnetic elements, the major contribution to ΔS_{sol} arises from lattice vibrations. We defer a discussion of the calculation of vibrational properties to a future paper.

IV. RESULTS

A. Promotion energies of elements

We begin the discussion of our results with the promotion energies for the pure elements. For each of the twenty-six elements X, we calculated energetics for X in each of the following crystal structures: fcc, bcc, hcp, β-Sn, diamond cubic, and body-centered tetragonal (bct). The ground state structures for these elements are given in Table I. For elements where the observed ground state falls outside this set (Ga, Sb, Bi, Mn), the observed ground state structure was also calculated.

For Ni, Co, Fe, Mn, and Cr, spin-polarized magnetic calculations were also performed in ferromagnetic (FM) geometries. For Cr, antiferromagnetic (AFM) calculations were also performed (see below). Note that in all cases, the somewhat arbitrary decision is made to define the promotion energy with respect to *nonmagnetic* (NM) fcc state. In other words, the promotion energy for magnetic materials includes not only the structural energy involved in promoting from the equilibrium geometry to the fcc geometry, but also the magnetic energy in going from magnetic to nonmagnetic states. Thus, even for metals like Ni that have an fcc ground state, there is a "promotion energy" associated with the development of a ferromagnetic ground state (0.04 eV).

In all cases, we find that the observed ground state was most energetically favorable with two caveats: (1) For the alkali and alkaline earth metals considered here, e.g., Li, Mg, and Sr, the fcc/hcp or fcc/bcc energy differences are extremely small, often less than 0.01 eV/atom. For the purposes of this paper, these tiny ($<$0.01 eV) energy differences are not important to resolve further, and thus we simply consider these competing ground states as "degenerate" (i.e., with a promotion energy of zero). (2) The commonly-used local density approximation (LDA) to DFT proves qualitatively deficient in the case of the magnetic metal, Fe, in that it leads to the prediction of an incorrect ground state, hcp nonmagnetic, rather than the observed bcc ferromagnetic state.[28] However, it has also been shown[29–31] that the correct

TABLE II. Comparison between LDA and GGA calculations for several solute elements in Al. In this table, all impurity energies are from 32-atom supercells. All energies are in eV/solute atom. For solutes X=Mn and Fe, the ordered compounds in this table refer to Al_6Mn and $Al_{13}Fe_4$, respectively.

Solute	ΔH_{imp}^{fcc}		ΔH_{promo}				ΔH_{imp}^{eq}		ΔH_{ord}^{eq}		$\Delta H_{solub.}$	
	LDA	GGA	LDA		GGA		LDA	GGA	LDA	GGA	LDA	GGA
			ΔH	Ground state	ΔH	Ground state						
Vacancy	+0.69	+0.54					+0.69	+0.54				
Cr	−0.40	−0.43	+0.41	bcc-NM	+0.43	bcc-AFM	+0.01	−0.00	−0.92	−0.90	−0.93	−0.90
Mn	−0.38	−0.44	+0.09	α-Mn	+0.08	α-Mn	−0.29	−0.36	−1.27	−1.29	−0.98	−0.93
Fe	−0.60	−0.66	+0.09	hcp-NM	+0.25	bcc-FM	−0.51	−0.41	−1.52	−1.36	−1.01	−0.95
Co	−0.91	−0.96	+0.09	hcp-FM	+0.23	hcp-FM	−0.82	−0.73	−2.01	−1.84	−1.19	−1.11
Ni	−0.89	−0.92	+0.04	fcc-FM	+0.06	fcc-FM	−0.85	−0.86	−1.77	−1.68	−0.92	−0.82
Si	−0.12	−0.13	+0.47	diamond	+0.62	diamond	+0.35	+0.49	0.00	0.00	−0.35	−0.49
Ge	+0.02	+0.07	+0.31	diamond	+0.35	diamond	+0.33	+0.42	0.00	0.00	−0.33	−0.42
Ga	+0.00	+0.12	+0.05	α-Ga	+0.03	α-Ga	+0.05	+0.15	0.00	0.00	−0.05	−0.15

ground state is recovered by use of the generalized gradient approximation (GGA).

LDA vs *GGA values*: To further investigate this distinction between ground-state stability within LDA and GGA, we have performed a comparison of these two exchange correlations for several solute elements. The results are shown in Table II. For the pure elements, in addition to the ground state of Fe being affected by the choice of LDA vs GGA, a difference in ground state stability is also found for Cr. The observed antiferromagnetic (AFM) state of Cr involves a complex magnetic structure; for simplicity, we used a CsCl-type $B2$ cell for the magnetic ordering. In the case of GGA, this structure converged to an AFM spin-polarized solution with an energy lower than the nonmagnetic (NM) bcc state, whereas in the LDA calculations, the Cr AFM calculation converged to a NM state. These results are consistent with previous LDA and GGA investigations of Cr.[32–34] In addition to the qualitative distinction found for Cr and Fe, a quantitative difference in promotion energy was found for the case of hcp-FM Co, with a much larger promotion energy in GGA calculations than in the LDA. Another quantitative dissimilarity was found for the promotion energy of Si from the tetrahedrally-bonded diamond phase to the close-packed fcc phase. Again, GGA calculations provided a larger promotion energy than the LDA. We note that GGA consistently provides energies in better agreement with observed stability: in the cases of Fe and Cr, GGA (LDA) provides the correct (incorrect) ground states. Additionally, in the case of Si, recent work has demonstrated that the quantitatively larger promotion energy in GGA leads to a more accurate prediction of Si solubility in Al.[35]

US vs *PAW potentials*: We have also investigated the differences between the energetics from US and PAW potential calculations. The results of this comparison are shown in Table III. In general, we note quite similar results for the two sets of potentials, with the one exception being the case of Fe. The promotion energy of Fe from the bcc-FM state to the fcc-NM state is much larger in the US calculations than in PAW. The latter result is consistent with a recent study of promotion energies using VASP and PAW.[36] Note, however,

TABLE III. Comparison between US and PAW (GGA) calculations for several solute elements in Al. The calculations using US potentials are as described in the text, using a cutoff of 237 eV, whereas the PAW calculations use 350 eV. All energies are in eV/solute atom. The calculated impurity energies given here are for 64-atom supercells. For solutes X=Ti, V, Mn and Fe, the ordered compounds in this table refer to Al_3Ti ($D0_{22}$), $Al_{10}V$, Al_6Mn, and $Al_{13}Fe_4$, respectively. All results are GGA, unless otherwise indicated.

	ΔH_{promo}		ΔH_{imp}^{eq}		ΔH_{ord}^{eq}	
Solute	US	PAW	US	PAW	US	PAW
Ti	+0.05(LDA)	+0.06	−1.26(LDA)	−1.18	−1.70(LDA)	−1.60
V	+0.31(LDA)	+0.25	−0.63(LDA)	−0.66	−1.01(LDA)	−1.14
Mn	+0.08	+0.08	−0.36	−0.33	−1.29	−1.26
Fe	+0.25	+0.10	−0.33	−0.46	−1.36	−1.62
Co	+0.23	+0.16	−0.62	−0.68	−1.84	−1.92
Ni	+0.04(LDA)	+0.05	−0.78(LDA)	−0.80	−1.77(LDA)	−1.71
Cu	+0.00	+0.00	−0.08(LDA)	−0.12	−0.56(LDA)	

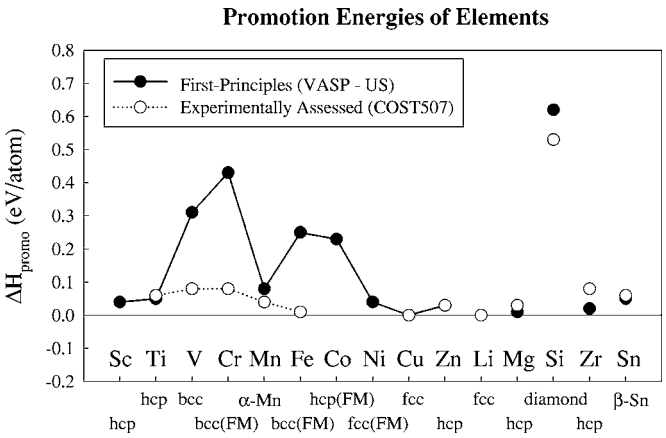

FIG. 1. First-principles VASP calculated and COST507 values (Ref. 10) of promotion energies of pure elements. The promotion energies are defined by Eq. (7) as the energy required to promote the element from its equilibrium crystal structure (indicated in the figure) to a nonmagnetic fcc structure. Note that VASP results in this figure are all calculated using US potentials; the promotion energy for Fe for PAW potentials is substantially reduced (see Table III).

that to maintain consistency, all figures and tables (other than Table III) contain only US results.

We next turn to a comparison of our first-principles results for promotion energies with those from the COST507 database. This comparison is shown in Fig. 1. In addition, in order to facilitate a detailed, quantitative comparison, we have also collected these promotion energy results along with those of ordered compounds and dilute impurities into Table IV. We note that the magnetic contribution to the promotion energy in the COST507 database is not included in the comparisons here, though this contribution is generally small.

From Fig. 1 and Table IV, we see that the comparison between first-principles and COST507 promotion energies is generally quite good, with the notable exception of V, Cr, and Fe, all bcc metals. This discrepancy between first-principles and CALPHAD promotion energies for fcc/bcc energy differences has been noted previously by many authors.[8,37] The reason for the discrepancy is due to the mechanical instability of the fcc phase in bcc metals, and of the bcc phase in fcc metals, as predicted in the first-principles calculations.[38] These instabilities lead to difficulties in even defining the entropic contribution to the promotion energy, and therefore the comparison between $T=0$ K first-principles promotion energies and finite-temperature CALPHAD energetics is not straightforward. However, despite the fact that the source of this discrepancy was discovered nearly a decade ago, a general solution to the instability problem remains elusive. The large promotion energy of hcp Co from the first-principles does not stem from an instability, as in the case of the bcc metals, but rather simply from our choice of reference state (the nonmagnetic fcc structure): Co gains much energy from spin polarization (0.21 eV/atom) and thus, while the promotion energy between the FM-hcp and NM-fcc structures is large, $E^{\text{NM-fcc/FM-hcp}}=0.23$ eV/atom, the promotion energy between FM-hcp and FM-fcc is much smaller, $E^{\text{FM-fcc/FM-hcp}}=0.02$ eV/atom.

B. Compound formation enthalpy

The calculated formation enthalpies for Al-rich compounds are given in Fig. 2 as well as Table IV. Again, we note that the Al-rich intermetallics form a rich variety of structure types, and therefore provide a critical test of computational methods. We have also given a comparison between LDA and GGA formation enthalpies in Table II. We note that the choice of LDA vs GGA does not make a large quantitative difference in many of the compound energies. However, Al-Fe and Al-Co show some LDA/GGA distinction that can largely be traced back to the differences in promotion energies for Fe and Co discussed above.

We also provide a comparison between first-principles and COST507 formation enthalpies[10] for ordered compounds in Fig. 2 and Table IV. The comparison is generally very good, with differences often within about 10%. This excellent agreement with COST507 for the ordered compounds is interesting, since more reliable experimental data are typically available for ordered compounds, and thus one might suppose that the COST507 database is more accurate for these phases. Thus, this comparison gives us confidence in the first-principles predictions not only for the ordered compounds, but also for the impurity cells, even in cases where there are quantitative differences with COST507. It is somewhat surprising that the greatest source of discrepancy between first-principles and COST507 is for Ti and Zr, whose ordered compounds, Al_3Ti and Al_3Zr, in some sense are the "simplest" compounds considered: fcc-based close-packed structures. We note that first-principles as well as experimental and CALPHAD energetics of compounds in the Al-Ti and Al-Zr systems have recently been thoroughly reviewed by Ghosh and Asta.[39] These authors show[39] that there is a significant spread in the experimental calorimetry measurements and the CALPHAD assessed values for ΔH in Al_3Ti and Al_3Zr. The COST507 values quoted in Fig. 2 are much less negative than most other experimental/assessed values. In contrast, our first-principles values are largely consistent with the previous first-principles calculations, with GGA energetics being slightly less negative than LDA results. Thus, the uncertainty in the experimental/assessed values is more than wide enough to explain the relatively large discrepancy with the first-principles values in Fig. 2.

Figure 2 illustrates an interesting trend in the Al-X, $X=3d$ transition metal series. The formation energies are all strongly negative (favoring ordered compounds) for all transition metals, particularly so for transition metals with partially filled bands. As the $3d$ state fills and one approaches $X=$Cu, the ordering tendency decreases. Towards the middle of the $3d$ series, the formation enthalpies show a maximum near $X=$Cr, whereas the most pronounced ordered tendency falls towards the "early" or "late" transition metals $X=$Sc, Ti, Co, and Ni. Interestingly, this same general trend was noted by Carlsson[40] in the context of analyzing ordering tendencies of Al alloys on an fcc lattice. He attributed the observed trends in formation enthalpies to the variation in the d electron count and in the second and fourth moments of the transition metal d electron density of states. In his study, Carlsson used augmented-spherical wave (ASW) calculations neglecting full potential, magnetic, and atomic relax-

TABLE IV. First-principles energetics of binary aluminum alloys. Impurity formation enthalpies, promotion energies, ordered formation enthalpies, and solubility enthalpies are all given in eV/solute atom, and compared with the COST507 CALPHAD database.[10] Note that all first-principles calculations are done using the LDA except for solutes X=Si, Cr, Mn, Fe, Co, Ge, Ga, which are GGA. The calculated impurity energies given here are for 64-atom supercells.

	$\Delta H_{\text{imp}}^{\text{fcc}}$		ΔH_{promo}		$\Delta H_{\text{imp}}^{\text{eq}}$		$\Delta H_{\text{ord}}^{\text{eq}}$		$\Delta H_{\text{solub.}}$		
Solute	VASP	COST507	VASP	COST507	VASP	COST507	VASP	COST507	VASP	COST507	Hatch
Vacancy	+0.67				+0.67		0.00		−0.67		
Li	−0.38	−0.25	0.00	0.00	−0.38	−0.25	−0.41	−0.43	−0.03	−0.18	−0.28
Mg	+0.04	+0.07	+0.01	+0.03	+0.05	+0.10	−0.05	−0.04	−0.10	−0.14	−0.19
Si	−0.12	−0.03	+0.62	+0.53	+0.50	+0.50	0.00	0.00	−0.50	−0.50	−0.51
Sc	−1.23		+0.04		−1.19		−1.96		−0.77		−0.72
Ti	−1.31	−1.18	+0.05	+0.06	−1.26	−1.12	−1.70[a], −1.74[b]	−1.50[a]	−0.44[a]	−0.38	−0.66
V	−0.94	−0.81	+0.31	+0.08	−0.63	−0.73	−1.01[c], −1.16[d], −1.14[e]	−1.15[c], −1.13[d], −1.08[e]	−0.38[c]	−0.39	−0.76
Cr	−0.57	−0.48	+0.43	+0.08	−0.14	−0.40	−0.90	−0.90	−0.76	−0.50	−0.70
Mn	−0.44	−0.63	+0.08	+0.04	−0.36	−0.59	−1.29[f], −1.38[g]	−1.29[f], −1.30[g]	−0.93[f]	−0.70	−0.63
Fe	−0.58	−0.57	+0.25	+0.01	−0.33	−0.56	−1.36[h], −1.37[i], −1.31[j]	−1.35[h]	−1.03[h]	−0.79	−0.99
Co	−0.85		+0.23		−0.62		−1.84		−1.22		
Ni	−0.82		+0.04	0.00	−0.78		−1.77		−0.99		−0.99
Cu	−0.08	−0.14	0.00	0.00	−0.08	−0.14	−0.56	−0.49	−0.48	−0.35	−0.42
Zn	+0.08	+0.11	+0.03	+0.03	+0.11	+0.14	0.00	0.00	−0.11	−0.14	−0.09
Ga	+0.09		+0.03		+0.12		0.00		−0.12		−0.20
Ge	+0.07		+0.35		+0.42		0.00		−0.42		−0.42
Sr	+1.04		0.00		+1.04		−1.25		−2.29		
Zr	−1.32	−1.19	+0.02	+0.08	−1.30	−1.11	−2.07	−1.68	−0.77	−0.57	−0.89
Ag	+0.02		0.00		+0.02		−0.23		−0.25		−0.28
Cd	+0.52		+0.01		+0.53		0.00		−0.53		−0.85
In	+0.66		0.00		+0.66		0.00		−0.66		
Sn	+0.72	+0.47	+0.05	+0.06	+0.77	+0.53	0.00	0.00	−0.77	−0.53	
Sb	+0.67		+0.29		+0.96		−0.30		−1.26		
Ba	+2.28		+0.01		+2.29		−1.45		−3.74		
Au	−0.58		0.00		−0.58		−1.34		−0.76		−0.91
Pb	+1.56		+0.00		+1.56		0.00		−1.56		
Bi	+1.46		+0.15		+1.61		0.00		−1.61		

[a] Al_3Ti-$D0_{22}$.
[b] Al_3Ti-$D0_{23}$.
[c] $Al_{10}V$.
[d] $Al_{45}V_7$.
[e] Al_3V-$D0_{22}$.
[f] Al_6Mn.
[g] $Al_{12}Mn$.
[h] $Al_{13}Fe_4$.
[i] Al_6Fe.
[j] Al_9Fe_2.

ation effects. In contrast, our current results are not confined to fcc geometries, contain a vast array of structure types, and use considerably more accurate first-principles techniques than this previous study (including a full potential approach and incorporating atomic relaxation). Yet despite these differences, we still see a trend across the transition metal series that is very similar to the one calculated by Carlsson. The robustness of this trend thus suggests that it is not sensitive to details of structure type and atomic environments, but rather is controlled largely by electronic structure considerations, as Carlsson argued.[40] We see below that a similar trend holds for the very different structural geometries involved in the impurity energies and mixing energies, further validating Carlsson's claims.

For several of the systems considered, more than one ordered compound was investigated:

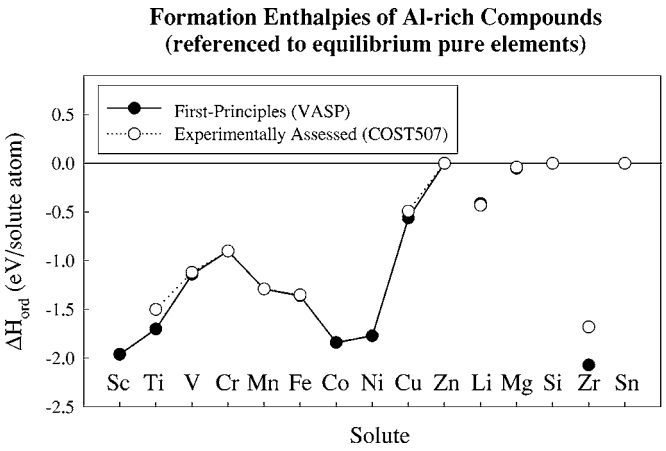

FIG. 2. Formation enthalpies of Al-rich ordered compounds with respect to constitutents in their equilibrium structures. The first-principles calculated values are compared with those from the COST507 assessment (Ref. 10). The equilibrium compounds for each system are given in Table I.

(1)*Al-Ti*. Though the Al_3Ti compound is reported to exist in the $D0_{22}$ structure at high temperature, there are reports of a long-period $D0_{22}$-based structure at low temperature. In a first-principles study, Amador *et al.*[41] found that Al_3Ti in the $D0_{23}$ structure (which can be considered an antiphased version of $D0_{22}$) actually is lower in energy than $D0_{22}$. Our present calculations confirm this finding, with $D0_{23}$ lower in energy than $D0_{22}$ by 0.04 eV/Ti atom (Table IV).

(2)*Al-V*. The Al-rich portion of the Al-V phase diagram contains several intermetallic compounds, with stoichiometries Al_3V, $Al_{45}V_7$, and $Al_{10}V$, among others. We have calculated the energies of all three competing Al-V compounds. Since all three exist in the observed Al-V phase diagram, one might expect that they are all ground states, and therefore their formation energies, when plotted as a function of composition, would fall on the "convex hull" of ground states. Or, put another way, the most Al-rich compound on the convex hull will have the most negative formation enthalpy, when expressed in energy per solute atom. From our results in Table IV, we see that the formation energy per solute atom of $Al_{45}V_7$ is slightly lower than Al_3V (indicating that both phases can be on the ground state hull), however, the energy of $Al_{10}V$ is above $Al_{45}V_7$. This energetic ordering is surprising, as it means that the energy of $Al_{10}V$ falls above the tie-line connecting $Al_{45}V_7$+Al, and does not fall on the ground state hull. The observed stability of $Al_{10}V$ could therefore be due to entropic considerations.

(3)*Al-Mn*. The Al-rich portion of the Al-Mn phase diagram has compounds with stoichiometries Al_6Mn and $Al_{12}Mn$. From our calculations of both these phases, we find that per Mn atom, $Al_{12}Mn$ has a lower energy than Al_6Mn, indicating that both can be on the ground state hull for this system.

(4)*Al-Fe*. The observed phase diagram shows an Al-rich compound, $Al_{13}Fe_4$. However, two metastable phases are known to form in this system by quenching from the liquid state: The Al_6Fe phase (isostructural with Al_6Mn) forms easily during quenching, whereas Al_9Fe_2 (isostructural with Al_9Co_2) is formed only upon very fast quenching.[42] Our calculations of these three phases (Table IV) show that the equilibrium $Al_{13}Fe_4$ and "easy-to-form" metastable Al_6Fe phases are nearly degenerate in energy (per Fe atom), indicating that the Al_6Fe is nearly degenerate in energy with a two-phase mixture of $Al_{13}Fe_4$+Al. This near degeneracy could explain the relative ease of formation of the metastable phase. On the other hand, the "hard-to-form" Al_9Fe_2 phase is considerably higher in energy than the equilibrium phase, consistent with the requirement of rapid quenching necessary for formation of this compound.

In the Al-Ag system, no ordered compounds are reported in Ref. 3, but rather only fcc, hcp, and bcc solution phases. In this system, we have simply performed calculations for ~20 fcc-based phases, such as the ones used in the construction of cluster expansions. See Ref. 43 for a description of these phases. Out of these 20 structures, one structure emerged as quite low in energy: an Al_2Ag_2 superlattice stacked along [110] (referred to as "Y2" in Ref. 43). This hypothetical AlAg "Y2" structure was used in the plots and tables here.

C. Dilute heat of mixing

The dilute heat of mixing was computed by considering fcc supercells with a single, substitutional solute impurity. Calculations were performed for 32- and 64-atom supercells, and the results are compared in Table V. From this table, we see that for many solutes, the dilute heat is already reasonably converged with a 32-atom cell. However, for some transition metal impurities (e.g., Ti, V) there is a sizable distinction between the 32- and 64-atom results. Zou and Carlsson[44] have pointed out that for these early transition-metal impurities in Al, Friedel oscillations lead to a long-range oscillating tail in the effective pair potentials, often extending beyond two lattice constants (the linear dimension of the 32-atom impurity cell). Direct first-principles calculations of the electronic charge density perturbation around a Sc impurity in Al using large supercells confirm the long-ranged nature of these effects.[45]

Table II shows a comparison between LDA and GGA calculated impurity energies for a few solutes. Although there are some small quantitative differences, there are no qualitative distinctions between LDA/GGA impurity heats, as was the case for promotion energy and ground state stability. Interestingly, the largest difference between LDA and GGA comes for the case of the isoelectronic solute impurity, Ga.

In Table IV and Figs. 3 and 4, we compare the first-principles calculated dilute mixing energies with those from the COST507 database. Figure 3 shows the dilute heat of mixing referenced to the pure elements in their equilibrium structures, while Fig. 4 shows the dilute heat with respect to the pure elements in their fcc structures. Although there are many examples of systematic comparisons of first-principles and experimental ordered compound energetics, such a comparison for dilute impurities is more rare. The comparisons between first-principles and COST507 in Figs. 3 and 4 show a good agreement for the dilute impurity energies, though the comparison is not quantitatively as accurate as for the or-

TABLE V. First-principles mixing energies of binary aluminum alloys. Given are impurity energies for 32- and 64-atom cells, as well as Al_3X, AlX, and AlX_3 SQS-16 energies. The final two columns represent the polynomial coefficients, L^0 and L^1, in a third-order fit to these mixing energies.

Solute	$\Delta H_{\text{imp}}^{\text{fcc}}$ (per solute) 64-atom	$\Delta H_{\text{imp}}^{\text{fcc}}$ (per solute) 32-atom	$\Delta H_{\text{mix}}^{\text{fcc}}(A_3B)$ (per solute)	$\Delta H_{\text{mix}}^{\text{fcc}}(A_3B)$ (per atom)	$\Delta H_{\text{mix}}^{\text{fcc}}(AB)$ (per atom)	$\Delta H_{\text{mix}}^{\text{fcc}}(AB_3)$ (per atom)	L^0	L^1
Li	−0.38	−0.37	−0.27	−0.067	−0.117	−0.138	−0.503	+0.254
Mg	+0.04	+0.045	+0.044	+0.011	+0.020	+0.003	+0.060	+0.004
Si(LDA)		−0.12	−0.11	−0.028	−0.074	−0.104		
Si(GGA)	−0.12	−0.13	−0.12	−0.029	−0.103	−0.144	−0.433	+0.483
Sc	−1.23	−1.19	−0.88	−0.220	−0.374	−0.232	−1.358	+0.219
Ti	−1.31	−1.10	−0.93	−0.232	−0.373	−0.275	−1.426	+0.315
V	−0.94	−0.69	−0.65	−0.163	−0.310	−0.334	−1.278	+0.762
Cr(LDA)	−0.57	−0.40	−0.40	−0.100	−0.260	−0.314		
Cr(GGA)		−0.43	−0.46	−0.116	−0.262	−0.402	−1.201	+1.124
Mn(LDA)		−0.38	−0.31	−0.078	−0.148	−0.108		
Mn(GGA)	−0.44	−0.44	−0.64	−0.159	−0.189	−0.176	−0.824	+0.151
Fe(LDA)		−0.60	−0.46	−0.115	−0.228	−0.107		
Fe(GGA)	−0.58	−0.66	−0.66	−0.164	−0.333	−0.263	−1.240	+0.630
Co(LDA)		−0.91	−0.97	−0.242	−0.400	−0.275		
Co(GGA)	−0.85	−0.96	−0.98	−0.246	−0.404	−0.337	−1.588	+0.566
Ni(LDA)	−0.82	−0.89	−1.06	−0.264	−0.518	−0.419	−1.954	+1.030
Ni(GGA)		−0.92	−1.05	−0.262	−0.498			
Cu	−0.08	−0.10	−0.21	−0.053	−0.099	−0.152	−0.467	+0.416
Zn	+0.08	+0.08	+0.05	+0.012	+0.012	+0.001	+0.042	+0.048
Ga(LDA)	+0.00	+0.00						
Ga(GGA)	+0.09	+0.12						
Ge	+0.07	+0.07						
Sr	+1.04	+0.88						
Zr	−1.32	−1.11	−0.95	−0.236	−0.359	−0.245	−1.364	+0.178
Ag	+0.02	0.00	−0.10	−0.024	−0.055	−0.086	−0.254	+0.280
Cd	+0.52	+0.50						
In	+0.66	+0.64						
Sn	+0.72	+0.68						
Sb	+0.67	+0.63						
Ba	+2.28	+2.00						
Au	−0.58	−0.63						
Pb	+1.56	+1.49						
Bi	+1.46	+1.38						

dered compounds (where, as we argue above, presumably better experimental data are available).

The differences between the quantity plotted in Figs. 3 and 4 are simply given by the promotion energies of the elements. And, given that the fcc/bcc instability issue causes large distinctions in promotion energies for some bcc metals, we wish to see how these promotion energy distinctions affect the comparison between first-principles and COST507 for $\Delta H_{\text{imp}}^{\text{fcc}}$ vs $\Delta H_{\text{imp}}^{\text{eq}}$. Interestingly, the distinction in promotion energies seems to be roughly split between $\Delta H_{\text{imp}}^{\text{fcc}}$ and $\Delta H_{\text{imp}}^{\text{eq}}$. In Fig. 3, we see that the comparison between first-principles and COST507 for $\Delta H_{\text{imp}}^{\text{eq}}$ shows that the first-principles values are higher than COST507 for the bcc metals V and Cr. However, in Fig. 4, we see just the opposite for $\Delta H_{\text{imp}}^{\text{fcc}}$, where the first-principles values are lower than those from COST507.

The trend in the heat of mixing across the $X=3d$ transition metal series is similar to that obtained from the ordered compound formation enthalpies: The heats of mixing in Figs. 3 and 4 are all strongly negative across this series, with the strongest negative values for the early transition metals, Sc and Ti, and the late ones, Co and Ni. However, in the ordered compounds, the magnitudes of the formation enthalpies for the early and late transition metals are comparable (i.e., the Co and Ni compounds have a similar ΔH_{ord} to the Sc compound), while for the dilute mixing energies, the early tran-

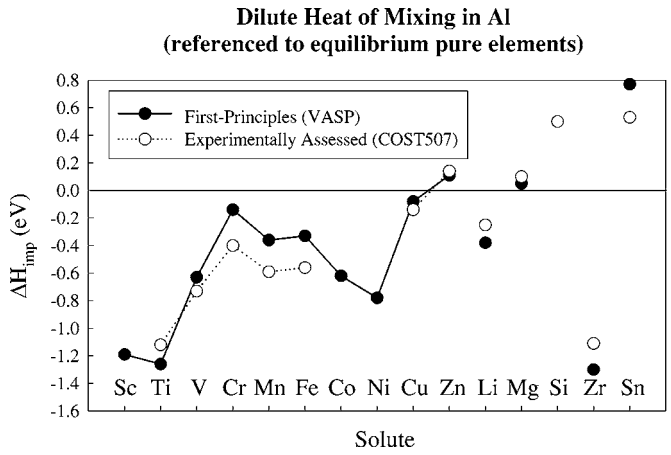

FIG. 3. Dilute heat of mixing with respect to constitutents in their equilibrium structures. The first-principles calculated values from 64-atom impurity supercells are compared with those from the COST507 assessment (Ref. 10).

sition metals, Sc and Ti, clearly have a more negative ΔH_{imp} than the late transition metals, Co and Ni. The general correlation of the trends for ordering vs mixing, as well as the distinction between the early and late transition metal behavior, will have an influence on the solubility enthalpies as described below.

We also note the peculiar behavior of the Li impurity (see Table IV): The impurity energy for Li is quite negative, and is almost equal to that of the ordered compound. Consequently, the difference between ordered and impurity enthalpies seems to be abnormally small. In an attempt to track down the source of the unusual energetics, calculations were performed using a "harder" Li potential, higher cutoffs, as well as PAW and PAW-GGA. These give similar energetics as the US-LDA results for the Al-Li ordered compounds. At present, the source of this unusual behavior of the Al-Li energetics in unclear. We also note that our results are quantitatively consistent with previous first-principles calculations of the impurity energy of Li in Al.[46]

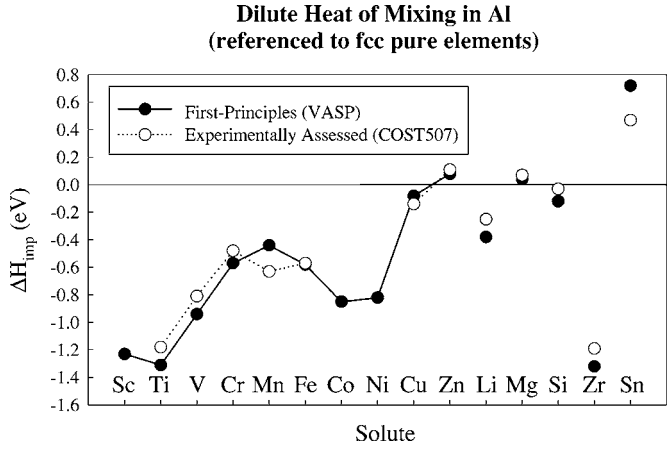

FIG. 4. Dilute heat of mixing with respect to fcc-based constitutents. The first-principles calculated values from 64-atom impurity supercells are compared with those from the COST507 assessment (Ref. 10).

D. Heat of mixing

In addition to the dilute impurity heat of mixing, we wish to ascertain the mixing energy for concentrated alloys as well. For this purpose, we rely on the "special quasirandom structure" (SQS) approach,[14] an efficient means to calculate random alloy properties within a small-unit-cell approach. We use fully relaxed, binary 16-atom SQS's, the structures of which are given fully in Appendix A of Ref. 26. For many (but not all) of the alloy systems considered here, we have computed SQS energetics with stoichiometries Al_3X, AlX, and AlX_3. The energetics of these SQS calculations are given in Table V.

In Table V, we compare the mixing energy per solute atom of the Al_3X SQS structures, with those from the 32- and 64-atom impurity supercells. Interestingly, despite the fact that this SQS structure is for a composition of $x=1/4$ and therefore is not very "dilute," the mixing energy of the Al_3X SQS provides a reasonable estimate of the dilute impurity energy for many solutes.

We have plotted the results of our SQS calculations, along with the impurity energies, the ordered compounds, and the pure elements in both equilibrium and fcc structures in Fig. 5. Tie lines are drawn to the Al-rich ordered compounds. The mixing energy results are fit to a third-order polynomial in concentration, analogous to the CALPHAD solution models of Eq. (5). The polynomial fit was weighted more heavily towards the Al-rich energetics, with each structure weighted by $1/x$ in the fit. The coefficients of this polynomial fit, L^0 and L^1, are also listed in Table V.

A few systems in Fig. 5 require comment: (1) For several Al-X systems (e.g., Al-Si, Al-V, Al-Cr, Al-Fe), the pure elements X are dynamically or mechanically unstable in the fcc state, as discussed above in Sec. IV A. In these systems, the atomic relaxations of the SQS structures tend to show signs of this instability, particularly as the composition becomes more solute rich. The SQS structures in some cases even fully relax to bcc-based topologies. Thus, for instance, the SQS energies of Al-V and Al-Cr in Fig. 5 can clearly be seen to extrapolate towards the bcc V, Cr, and Fe end point energies. Thus, these instabilities could cause errors in our polynomial fits, which by construction, have the fcc end points. (The choice of fcc end point is retained in order to facilitate the comparison with CALPHAD mixing energies with the analogous definition.) However, we are really mostly concerned with Al-rich composition, and correspondingly have fitted more heavily to these compositions. (2) For the solute elements X=Cr-Ni, spin-polarized calculations were performed for the SQS structures. This choice leads to a slight inconsistency in the mixing energies of Fig. 5 as the pure solute end points for these fits are the nonmagnetic fcc phases. However, the energetic effects of spin polarization were most pronounced for solute rich AlX_3 compositions which were weighted minimally in the polynomial fits.

We next wish to break down the contributions to the first-principles mixing energies into the types of parameters used in CALPHAD solution models, such as Eq. (5). In Fig. 6, we plot the second-order (L^0) and third-order (L^1) terms in the polynomial fits of the SQS energies in Fig. 5. From Eq. (5) we can see that L^0 scales directly with the size of the mixing

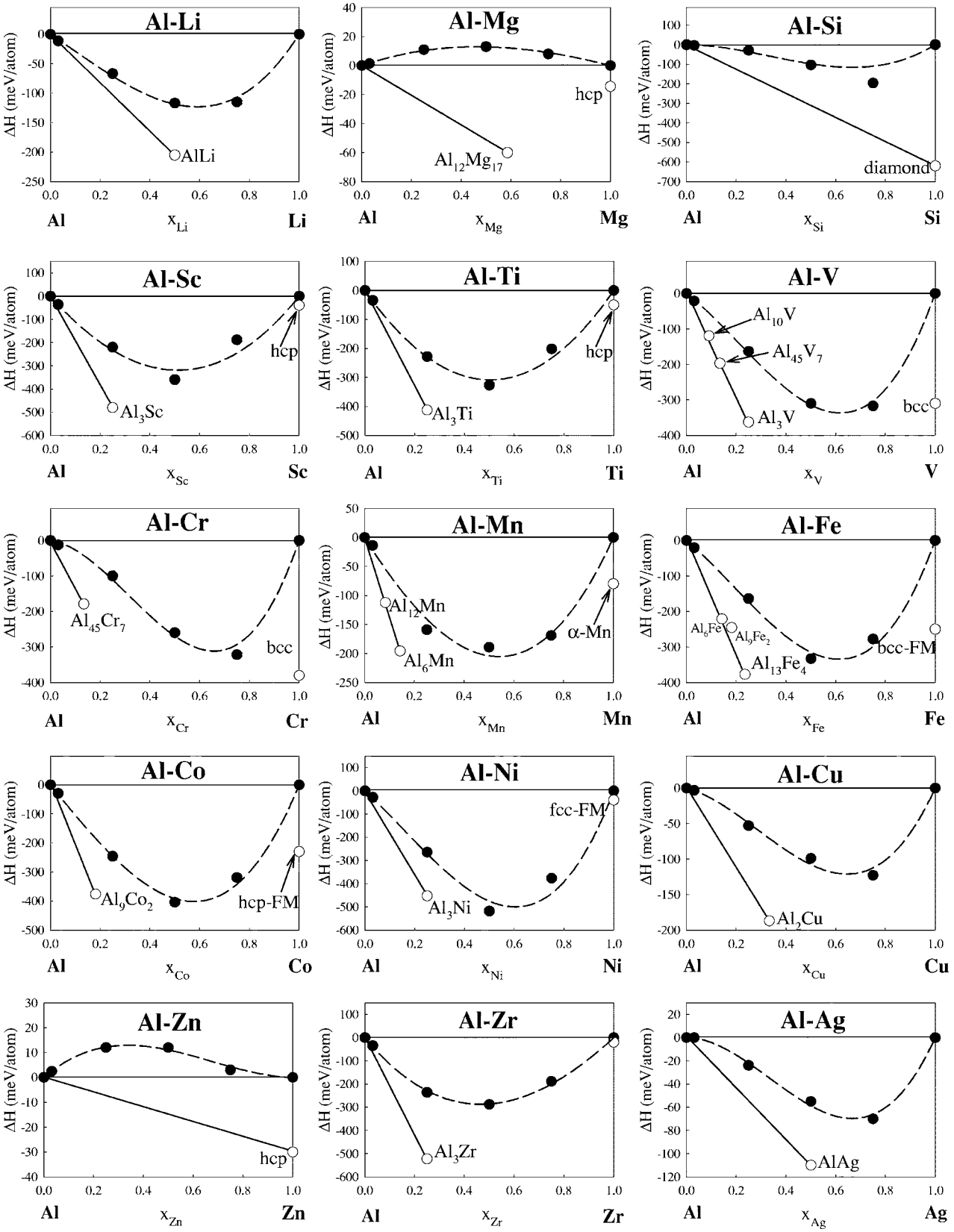

FIG. 5. Calculated energies of mixing and ordered compounds plotted as a function of composition for Al-*X* systems. The mixing energies were calculated using 16-atom SQS structures and fit to polynomials in solute concentration (dashed lines). Solid lines are tie-lines drawn between pure Al and the stable Al-rich compounds in each case.

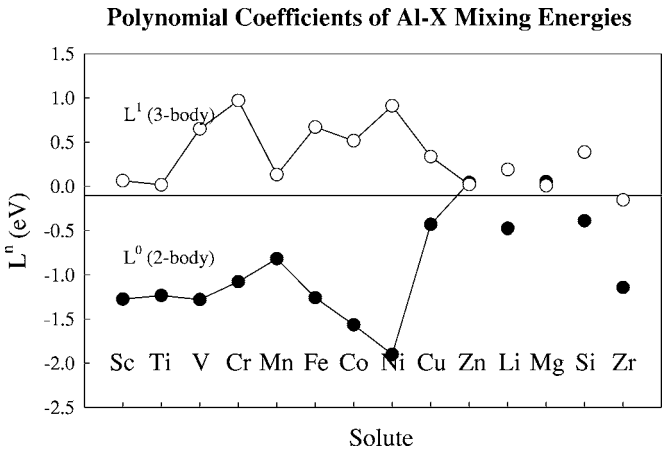

FIG. 6. Mixing energy solution parameters extracted from first-principles calculations. Shown are the polynomial coefficients from fits to the SQS formation energies shown in Fig. 5. L^0 represents the second-order fit (characterizing the size of the mixing energy at $x=1/2$), and L^1 is the third-order coefficient (characterizing the asymmetry in mixing energy between Al-rich and solute-rich regions).

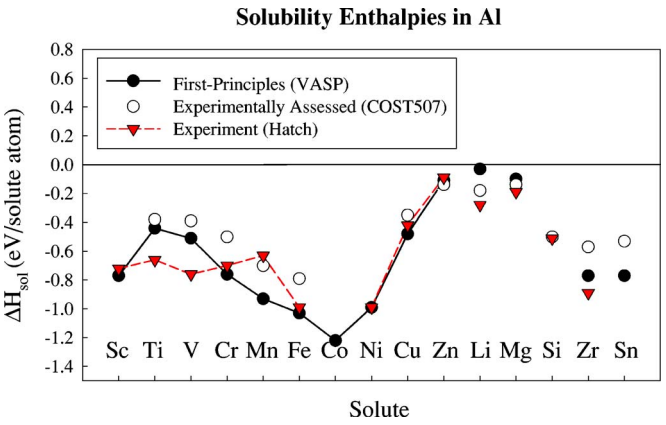

FIG. 7. (Color online) Solubility enthalpies ΔH_{sol} in Al. The solubility enthalpy represents the difference in enthalpy (per solute atom) between the disordered and ordered states. The first-principles values are derived from the difference in energies between the impurity supercell and ordered compound calculations. Also shown are the values from the COST507 assessment (Ref. 10), and also the values extracted directly from phase-diagram information, as described by Hatch (Ref. 1).

energy at $x=1/2$, and the third-order coefficient, L^1, gives a quantitative indication of the asymmetry in mixing energy about the point $x=1/2$.

Interesting trends emerge in the polynomial coefficients of Fig. 6: (1) The two-body or quadratic term in the mixing energy, L^0, simply scales with the overall "depth" of the mixing energy curve. As we see from Fig. 6, the general shape of L^0 along the $3d$ transition metal series is similar to that of the ordered compound enthalpies (Fig. 2) and the dilute impurity enthalpies (Figs. 3 and 4). The coefficients are all negative, with strongest ordering tendencies (most negative L^0) near the late transition metals, Co and Ni, and the early transition metals, Sc-V. (2) The three-body or cubic term in the mixing energy, L^1, measures the asymmetry of the mixing energy curve. Interestingly, from Fig. 6, we see that L^1 is almost always positive (Zr is the only slight exception), meaning that mixing energies are consistently more negative for solute-rich compositions than for Al-rich compositions.

E. Solubility energy

By taking the difference between the dilute heat of mixing and the ordered compound formation enthalpies, we can obtain the solubility energy ΔH_{sol} of Eq. (8). The results for ΔH_{sol} are shown in Fig. 7 for several solutes, and are given in Table IV for all solutes considered. This quantity is quite interesting, as it is directly related to the temperature dependence of the solubility, as in Eq. (9). For a given Al-X system, by fitting the measured solubility data as a function of temperature to Eq. (9), one can extract both ΔH_{sol} and ΔS_{sol}. Hatch[1] has done this for a series of Al-X systems, providing a method of extracting ΔH_{sol} directly from phase-diagram information. We note that the entropic contributions extracted from this procedure are sizable. In Fig. 7, we compare our first-principles values of the solubility energy ΔH_{sol} with those from the COST507 database, and also from Hatch's construction of measured phase diagram data. The comparison between first-principles and experiment is generally good, though there are some quantitative differences. However, it is worth noting that the disagreement between COST507 and Hatch is roughly of the same size as the disagreement with the first-principles values, suggesting that the experimental numbers could have significant uncertainties. The first-principles calculations again show the trend across the $3d$ series of strong negative values for early and late transition metals, with relatively strong negative values throughout the series. These strong negative values explain the relatively low solubility of most transition metals in Al. Higher solubilities are observed for systems like X=Cu, Zn, Li, Mg, Ag, Ga, all of which have much smaller values of the solubility energies.

In a future paper we will discuss the vibrational entropy contribution to solubility, as well as perform solubility calculations themselves for several solutes. The solubility itself provides a more critical test of our theoretical approach, since it is directly observable, as opposed to the solubility enthalpy and entropy, which can only be "inferred" from measurements.

V. SUMMARY

In summary, we have used density functional theory calculations to create a "first-principles aluminum database" of energetic properties for Al-X alloys and compounds. The binary systems examined include 26 solute elements, X=Li, Mg, Si, Sc, Ti, V, Cr, Mn, Fe, Co, Ni, Cu, Zn, Ga, Ge, Sr, Zr, Ag, Cd, In, Sn, Sb, Ba, Au, Pb, and Bi. For each of these Al-X systems, we have examined the energetics of ordered Al-rich compounds, dilute impurity supercells, concentrated random alloys (via the special quasirandom structure approach), as well as the pure elements X in both their equilib-

rium and other competing crystal structures. The first-principles energetics were compared extensively against the empirical data in the COST507 thermodynamic database.

We find:

(i) With the exception of the bcc metals, V, Cr, and Fe, the promotion energies required to promote the pure elements X from their equilibrium structure to a nonmagnetic fcc structure agree well with the values in the COST507 database. The discrepancy in the case of bcc metals is well known to be due to the mechanical instability of these bcc metals when placed in a hypothetical fcc structure.

(ii) The first-principles formation enthalpies of ordered compounds are in excellent quantitative agreement with COST507, even across a wide diversity of structure types, symmetries, unit cell sizes, and stoichiometries. First-principles impurity energies for X in Al also agree quantitatively well with the COST507 values, although not as well as in the case of ordered compounds.

(iii) The trends in formation enthalpies for Al-X systems across the $3d$ series are similar for ordered compounds as well as dilute impurity energies, despite the completely different local geometries in the ordered and impurity cases. The robustness of this trend tends to support previous studies which attribute these trends to generic electronic structure effects.

(iv) Using the SQS for compositions $x=1/4$, $1/2$, and $3/4$, fit to polynomials in concentration, the mixing energies for Al-X across the entire concentration range were deduced. From this construction, we find that the SQS energies can be used to accurately deduce the dilute impurity energies in many cases.

(v) In nearly all cases, the mixing energies of Al-X alloys are negative, and the systems form ordered compounds. Interestingly, in most systems considered, the sign of the *asymmetry* in the mixing energies is consistent, giving more negative mixing energies for X-rich compositions than in Al-rich compositions.

(vi) By taking the difference between the dilute impurity energetics and the ordered compound energetics, we obtain the solubility enthalpy, which is one of the key factors that describes the equilibrium solubility in these systems. The solubility enthalpies are nearly all strongly negative, consistent with the observation of very low solubility of X in many Al-X systems. A more complete discussion of solubility, including the role of entropic effects, will be given in a future paper.

The generally good agreement between the first-principles energetics and empirical databases of thermodynamic information provides confidence in the predictive abilities of this approach. Thus, this first-principles database should provide a good complement to the available CALPHAD thermodynamic databases for Al alloys (such as COST507). Additionally, the construction of such first-principles databases for materials where less information is currently available from experiment (e.g., Mg alloys) would therefore be of great value.

[1] J. E. Hatch, *Aluminum: Properties and Physical Metallurgy* (American Society of Metals, Metals Park, Ohio 1998).

[2] L. F. Mondolfo, *Aluminum Alloys—Struture and Properties* (Butterworths, London, 1976).

[3] T. B. Massalski, *Binary Alloy Phase Diagrams*, edited by J. L. Murray, L. H. Bennett, and H. Baker (ASM, Metals Park, Ohio, 1986).

[4] P. Villars and L. D. Calvert, *Pearson's Handbook of Crystallographic Data for Intermetallic Phases* (ASM, Metals Park, Ohio, 1991).

[5] P. Hohenberg and W. Kohn, Phys. Rev. **136**, B864 (1964); W. Kohn and L. J. Sham, Phys. Rev. **140**, A1133 (1965).

[6] L. Kaufmann and H. Bernstein, *Computer Calculation of Phase Diagrams* (Academic Press, New York, 1970).

[7] See the collection of articles in the *MRS Bulletin*, edited by P. J. Spencer, Vol. 24, April 1999.

[8] N. Saunders and A. P. Miodownik, *CALPHAD: Calculation of Phase Diagrams, A Comprehensive Guide* (Pergamon, New York, 1998).

[9] C. Wolverton, X.-Y. Yan, R. Vijayaraghavan, and V. Ozoliņš, Acta Mater. **50**, 2187 (2002).

[10] *COST507: Thermodynamic Database for Light Metal Alloys*, Vol. 2, edited by I. Ansara, A. T. Dinsdale, and M. H. Rand, July 1998, European Commision, rue de la Loi 200 (SDME 1/44), B-1049 Brussels. One should note that in this paper, COST507 values for $T=0$ were used whenever possible, rather than 298 K values. When the thermodynamic functions in COST507 contained inverse powers of T, then values at $T=298$ K were used. This distinction was used merely for simplicity.

[11] C. Wolverton and V. Ozoliņš, Phys. Rev. Lett. **86**, 5518 (2001).

[12] C. Wolverton, Philos. Mag. Lett. **79**, 683 (1999).

[13] V. Vaithyanathan, C. Wolverton, and L. Q. Chen, Phys. Rev. Lett. **88**, 125503 (2002).

[14] A. Zunger, S.-H. Wei, L. G. Ferreira, and J. E. Bernard, Phys. Rev. Lett. **65**, 353 (1990).

[15] G. Kresse and J. Hafner, Phys. Rev. B **47**, R558 (1993); G. Kresse, Thesis, Technische Universität Wien, 1993; G. Kresse and J. Furthmüller, Comput. Mater. Sci. **6**, 15 (1996); G. Kresse and J. Furthmüller, Phys. Rev. B **54**, 11169 (1996).

[16] D. Vanderbilt, Phys. Rev. B **41**, 7892 (1990).

[17] G. Kresse and J. Hafner, J. Phys.: Condens. Matter **6**, 8245 (1994).

[18] D. M. Ceperley and B. J. Alder, Phys. Rev. Lett. **45**, 566 (1980).

[19] J. P. Perdew and A. Zunger, Phys. Rev. B **23**, 5048 (1981).

[20] J. P. Perdew, in *Electronic Structure of Solids 1991*, edited by P. Ziesche and H. Eschrig (Akademie Verlag, Berlin, 1991), Vol. 11.

[21] S. Froyen, Phys. Rev. B **39**, 3168 (1989).

[22] H. J. Monkhorst and J. D. Pack, Phys. Rev. B **13**, 5188 (1976).

[23] N. Chetty, M. Weinert, T. S. Rahman, and J. W. Davenport, Phys. Rev. B **52**, 6313 (1995).

[24] D. E. Turner, Z. Z. Zhu, C. T. Chan, and K. M. Ho, Phys. Rev. B **55**, 13842 (1997).

[25] C. Wolverton, V. Ozoliņš, and M. Asta, Phys. Rev. B **69**, 144109

(2004).
[26] C. Wolverton, Acta Mater. **49**, 3129 (2001).
[27] C. Zener, in *Thermodynamics in Physical Metallurgy*, edited by C. Zener (ASM, Cleveland, OH, 1950), pp. 16–27.
[28] C. S. Wang, B. M. Klein, and H. Krakauer, Phys. Rev. Lett. **54**, 1852 (1985).
[29] J. Haglund, Phys. Rev. B **47**, R566 (1993).
[30] D. J. Singh, W. E. Pickett, and H. Krakauer, Phys. Rev. B **43**, 11628 (1991).
[31] C. Amador, W. R. L. Lambrecht, and B. Segall, Phys. Rev. B **46**, R1870 (1992).
[32] J. Chen, D. Singh, and H. Krakauer, Phys. Rev. B **38**, 12834 (1988).
[33] V. L. Moruzzi and P. M. Marcus, Phys. Rev. B **42**, 8361 (1990).
[34] D. J. Singh and J. Ashkenazi, Phys. Rev. B **46**, 11570 (1992).
[35] V. Ozoliņš, B. Sadigh, and M. Asta, J. Phys.: Condens. Matter **17**, 2197 (2005).
[36] Y. Wang, S. Curtarolo, C. Jiang, R. Arroyave, T. Wang, G. Ceder, L.-Q. Chen, and Z.-K. Liu, CALPHAD: Comput. Coupling Phase Diagrams Thermochem. **28**, 79 (2004).
[37] A. Fernandez Guillermet, V. Ozoliņš, G. Grimvall, and M. Korling, Phys. Rev. B **51**, 10364 (1995).
[38] P. J. Craievich, M. Weinert, J. M. Sanchez, and R. E. Watson, Phys. Rev. Lett. **72**, 3076 (1994).
[39] G. Ghosh and M. Asta, Acta Mater. **53**, 3225 (2005).
[40] A. E. Carlsson, Phys. Rev. B **40**, 912 (1989).
[41] C. Amador, J. J. Hoyt, B. C. Chakoumakos, and D. de Fontaine, Phys. Rev. Lett. **74**, 4955 (1995).
[42] C. M. Allen, K. A. Q. O'Reilly, B. Cantor, and P. V. Evans, Prog. Mater. Sci. **43**, 89 (1998).
[43] V. Ozoliņš, C. Wolverton, and A. Zunger, Phys. Rev. B **57**, 6427 (1998).
[44] J. Zou and A. E. Carlsson, Phys. Rev. B **47**, 2961 (1993).
[45] V. Ozoliņš and M. Asta, Phys. Rev. Lett. **86**, 448 (2001).
[46] M. H. F. Sluiter and Y. Kawazoe, Europhys. Lett. **57**, 526 (2002).